Frontiers of Information Technology & Electronic Engineering
www.jzus.zju.edu.cn; engineering.cae.cn; www.springerlink.com
ISSN 2095-9184 (print); ISSN 2095-9230 (online)
E-mail: jzus@zju.edu.cn

Affine formation tracking control of unmanned aerial vehicles*

Huiming LI, Hao CHEN, Xiangke WANG‡

College of Intelligence Science and Technology, National University of Defense Technology, Changsha 410073, China

E-mail: huiminglhm@163.com; chenhao09@nudt.edu.cn; xkwang@nudt.edu.cn

Received Feb. 28, 2021; Revision accepted Aug. 24, 2021; Crosschecked Jan. 25, 2022; Published online Mar. 29, 2022

Abstract: The affine formation tracking problem for fixed-wing unmanned aerial vehicles (UAVs) is considered in this paper, where fixed-wing UAVs are modeled as unicycle-type agents with asymmetrical speed constraints. A group of UAVs are required to generate and track a time-varying target formation obtained by affinely transforming a nominal formation. To handle this problem, a distributed control law based on stress matrix is proposed under the leader-follower control scheme. It is proved, theoretically, that followers can converge to the desired positions and achieve affine transformations while tracking diverse trajectories. Furthermore, a saturated control strategy is proposed to meet the speed constraints of fixed-wing UAVs, and numerical simulations are executed to verify the effectiveness of our proposed affine formation tracking control strategy in improving maneuverability.

Key words: Affine formation; Fixed-wing unmanned aerial vehicles; Multi-agent system
https://doi.org/10.1631/FITEE.2100109 **CLC number:** TP273

1 Introduction

With the rapid development of computation and communication capabilities, increasing attention has been paid to multi-agent systems for their huge potential value in industry, agriculture, national defense, and many other fields (Paranjape et al., 2018; Wang XK et al., 2019). For a widely applicable system with multiple unmanned aerial vehicles (UAVs), the ability to achieve various formations is critical.

In recent years, diverse formation control approaches have been proposed, including the leader-follower method (Miao et al., 2018; Chen H et al., 2021) and consensus theory (Ren et al., 2007; Zhao SY, 2018). Oh et al. (2015) divided existing formation control approaches based on consensus theory into three categories: displacement-, distance-, and bearing-based methods. The displacement-based formation control method uses the displacement constraints between agents to design control laws, so it is difficult to track target formations based on scale or orientation changes. Similarly, the distance-based control method can track target formations with time-varying translations and orientations instead of time-varying scales. The bearing-based control method performs well in tracking formations with time-varying translations and scales, rather than orientations. Consequently, these control methods have different problems related to solving the time-varying formation tracking problem (Lin ZY et al., 2016; Zhao SY, 2018). It is difficult to control the relative distance and position among agents without increasing the complexity of the protocol for these methods. As an alternative, an affine formation control scheme can drive the multi-agent system to track

‡ Corresponding author
* Project supported by the National Natural Science Foundation of China (No. 61973309), the Research Project of National University of Defense Technology, China (No. ZK21-05), and the Hunan Provincial Natural Science Foundation of China (No. 2021JJ10053)
ORCID: Huiming LI, https://orcid.org/0000-0002-5142-5151; Hao CHEN, https://orcid.org/0000-0002-7567-0063; Xiangke WANG, https://orcid.org/0000-0002-5074-7052
© Zhejiang University Press 2022

time-varying affine formation shape transformations, which enables the system to have better maneuverability in dynamic environments (Lin ZY et al., 2016; Zhao SY, 2018; Lin YJ et al., 2021).

The affine formation control scheme is inspired by affine transformation, which can deal with geometric distortions such as translation, rotation, scale, and their combinations. Therefore, the application of an affine formation control scheme provides a new way to track and reshape formations while preserving straightness and parallelism. Affine formation control strategies were proposed with different dynamic models, including the linear time-invariant model (Xu et al., 2018, 2019a; Onuoha et al., 2019a, 2019b; Chen LM et al., 2020), Euler-Lagrange model (Xu et al., 2019b, 2019c), and unicycle model with symmetrical constraints (Zhao SY, 2018; Xu et al., 2020). In Zhao SY (2018), some distributed controllers were designed based on the consensus protocol for agents described by the unicycle model. The convergence of the multi-agent system was achieved and analyzed, but the tracking control problem was not considered. In Xu et al. (2020), the affine formation tracking problem was taken into account. Agents can move along a straight line and achieve affine transformations in the process of trajectory tracking, but the inflexible trajectory tracking ability is not strong enough to meet the high-performance maneuverability requirements of fixed-wing UAVs.

In general, fixed-wing UAVs are usually described by the unicycle model, which is limited by asymmetrical input constraints. The classic model of small fixed-wing UAVs can be described by 12-dimensional, state-coupled, first-order ordinary differential nonlinear equations (Wu, 2013), and it is too complex to be directly used in guidance control problems. In the flight process, a minimum positive linear velocity, i.e., the stall speed, is necessary to generate sufficient lift for fixed-wing UAVs. In addition, the angular speeds have great influence on the UAVs' turning radius. Therefore, a simplified nonholonomic agent model, i.e., the unicycle model, is usually applied to describe fixed-wing UAV kinematics (Wang YZ et al., 2020; Zhao SL et al., 2020); its applicability has been proved in both simulations and flight experiments (Beard et al., 2014; Liu et al., 2020; Wang YZ et al., 2020; Zhao SL et al., 2020).

In this paper, we adopt the leader-follower strategy to solve the affine formation tracking control problem for the system with multiple fixed-wing UAVs. Theoretical analysis and simulation results are provided to illustrate the effectiveness of the proposed control strategy. The main contributions are as follows:

1. We propose an original distributed control law based on stress matrix to achieve the desired time-varying formation pattern and to track affine transformations along diverse trajectories, which improves the maneuverability of the fixed-wing UAV formation in dynamic environments.

2. The convergence of the distributed control law is analyzed for unicycle-type agents, which lays a foundation for the application of the affine formation control scheme in the system with multiple fixed-wing UAVs. In addition, a saturated control strategy is proposed to meet the asymmetrical speed constraints of fixed-wing UAVs, and the effectiveness is verified by numerical simulations.

2 Problem description

2.1 Notations of formations and graphs

Suppose that there are n fixed-wing UAVs in $\mathbb{R}^d$, where $d \geq 2$ and $n \geq d+1$. Denote $\boldsymbol{p}_i = [x_i, y_i]^{\mathrm{T}}$ the position of the ith UAV and $\boldsymbol{p} = [\boldsymbol{p}_1^{\mathrm{T}}, \boldsymbol{p}_2^{\mathrm{T}}, \cdots, \boldsymbol{p}_n^{\mathrm{T}}]^{\mathrm{T}} \in \mathbb{R}^{dn}$ the configuration of the whole UAV formation. Naturally, an undirected graph is used to model the communication topology among UAVs, i.e., $G = (\mathcal{V}, \mathcal{E})$, where $\mathcal{V} = \{1, 2, \cdots, n\}$ denotes the vertex set and $\mathcal{E} \subseteq \mathcal{V} \times \mathcal{V}$ denotes the edge set. The edge $(i, j) \in \mathcal{E}$ means that the ith UAV can receive information from the jth UAV. In the undirected graph, $(i, j) \in \mathcal{E} \Leftrightarrow (j, i) \in \mathcal{E}$. The neighbors of the ith UAV are defined as $\mathcal{N}_i = \{j \in \mathcal{V} : (i, j) \in \mathcal{E}\}$.

A formation is expressed as $(G, \boldsymbol{p})$ by associating the system with multiple fixed-wing UAVs and the undirected graph G. Inspired by the leader-follower control strategy, suppose that there are n_{l} UAVs playing the role of leaders and that the remaining n_{f} UAVs are followers, where $n_{\mathrm{f}} = n - n_{\mathrm{l}}$. Thus, the leader set is $\mathcal{V}_{\mathrm{l}} = \{1, 2, \cdots, n_{\mathrm{l}}\}$ and the follower set is $\mathcal{V}_{\mathrm{f}} = \mathcal{V} \backslash \mathcal{V}_{\mathrm{l}}$. Similarly, define $\boldsymbol{p}_{\mathrm{l}} = [\boldsymbol{p}_1^{\mathrm{T}}, \boldsymbol{p}_2^{\mathrm{T}}, \cdots, \boldsymbol{p}_{n_{\mathrm{l}}}^{\mathrm{T}}]^{\mathrm{T}}$ and $\boldsymbol{p}_{\mathrm{f}} = [\boldsymbol{p}_{n_{\mathrm{l}}+1}^{\mathrm{T}}, \boldsymbol{p}_{n_{\mathrm{l}}+2}^{\mathrm{T}}, \cdots, \boldsymbol{p}_n^{\mathrm{T}}]^{\mathrm{T}}$.

2.2 Stress matrix

A stress is a set of scalars that are assigned to all the edges, that is, ϖ_{ij} for $(i, j) \in \mathcal{E}$.

$\varpi_{ij} = \varpi_{ji}$ is reasonable for an undirected graph. For a formation $(G, \boldsymbol{p})$, an equilibrium stress (Connelly, 2005) is established only if the stress satisfies $\sum_{j\in\mathcal{N}_i} \varpi_{ij}(\boldsymbol{p}_j - \boldsymbol{p}_i) = \boldsymbol{0}$, which can be reworded in another form as

$$(\boldsymbol{\Omega} \otimes \boldsymbol{I}_d)\boldsymbol{p} = \boldsymbol{0}, \tag{1}$$

where "$\otimes$" represents the Kronecker product and $\boldsymbol{I}_d$ is the identity matrix. $\boldsymbol{\Omega} \in \mathbb{R}^{n\times n}$ is called the stress matrix satisfying

$$[\Omega]_{ij} = \begin{cases} -\varpi_{ij}, & i \neq j,\ \ j \in \mathcal{N}_i, \\ 0, & i \neq j,\ \ j \notin \mathcal{N}_i, \\ \sum_{k\in\mathcal{N}_i} \varpi_{ik}, & i = j. \end{cases} \tag{2}$$

Obviously, the stress matrix form is similar to the Laplacian matrix, while the weight in a stress matrix, ϖ_{ij}, may be positive, negative, or even zero.

2.3 Affine formation control

Geometrically, affine transformation means that a vector space is transformed into another vector space through a linear transformation followed by a translation. As shown in Fig. 1, affine transformations can realize rotation, translation, scaling, shear, and their combinations.

Similarly, a nominal configuration $\boldsymbol{r} = \left[\boldsymbol{r}_1^{\mathrm{T}}, \boldsymbol{r}_2^{\mathrm{T}}, \ldots, \boldsymbol{r}_n^{\mathrm{T}}\right]^{\mathrm{T}} = \left[\boldsymbol{r}_{\mathrm{l}}^{\mathrm{T}}, \boldsymbol{r}_{\mathrm{f}}^{\mathrm{T}}\right]^{\mathrm{T}} \in \mathbb{R}^{dn}$ is given as the affine transformation baseline of the fixed-wing UAV formation in $\mathbb{R}^d$. Thus, the nominal formation is expressed as $(G, \boldsymbol{r})$, and the time-varying target formation for $(G, \boldsymbol{p})$ is defined as follows:

Definition 1 (Target formation) The time-varying target formation has the form of

$$\boldsymbol{p}^*(t) = (\boldsymbol{I}_n \otimes \boldsymbol{A}(t))\,\boldsymbol{r} + \boldsymbol{1}_n \otimes \boldsymbol{b}(t), \tag{3}$$

where $\boldsymbol{1}_n = [1, 1, \cdots, 1]^{\mathrm{T}}$ and the variable with the superscript "$*$" represents the target value. The nominal configuration $\boldsymbol{r}$ is constant, while $\boldsymbol{A}(t) \in \mathbb{R}^{d\times d}$ and $\boldsymbol{b}(t) \in \mathbb{R}^d$ are continuous on t. In the target formation, the desired position of the ith UAV is expressed as $\boldsymbol{p}_i^*(t) = \boldsymbol{A}(t)\boldsymbol{r}_i + \boldsymbol{b}(t)$.

In fact, all the affine transformations of $\boldsymbol{r}$ are included in the affine image $\mathcal{A}(\boldsymbol{r})$ (Zhao SY, 2018), including the time-varying target formation $\boldsymbol{p}^*(t)$. In addition, for n fixed-wing UAVs in $\mathbb{R}^d$, define the affine span of $\{\boldsymbol{p}_i\}_{i=1}^n$ as

$$\mathcal{S} = \left\{\sum_{i=1}^n a_i\boldsymbol{p}_i : a_i \in \mathbb{R} \text{ for all } i \text{ and } \sum_{i=1}^n a_i = 1\right\},$$

which means that three non-collinear points can affinely span the two-dimensional (2D) plane. Without loss of generality, suppose that the nominal formation $(G, \boldsymbol{r})$ can meet the following condition:

Assumption 1 For nominal formation $(G,\ \boldsymbol{r})$, assume that $\{\boldsymbol{r}_i\}_{i=1}^n$ affinely span $\mathbb{R}^d$.

Based on the leader-follower control strategy, a notion termed affine localizability is defined to make clear that sufficient and appropriate leaders can guide the entire formation to the target affine formation.

Definition 2 (Affine localizability) (Zhao SY, 2018) The nominal formation $(G, \boldsymbol{r})$ is affinely localizable by the leaders if for any $\boldsymbol{p} = \left[\boldsymbol{p}_{\mathrm{l}}^{\mathrm{T}}, \boldsymbol{p}_{\mathrm{f}}^{\mathrm{T}}\right]^{\mathrm{T}} \in \mathcal{A}(\boldsymbol{r})$, $\boldsymbol{p}_{\mathrm{f}}$ can be uniquely determined by $\boldsymbol{p}_{\mathrm{l}}$.

Lemma 1 (Zhao SY, 2018) Under Assumption 1, the nominal formation $(G, \boldsymbol{r})$ is affinely localizable if and only if $\{\boldsymbol{r}_i\}_{i\in\mathcal{V}_{\mathrm{l}}}$ affinely span $\mathbb{R}^d$.

Lemma 1 means that UAVs in $(G, \boldsymbol{r})$ can be chosen as leaders to guarantee affine localizability as long as they can affinely span $\mathbb{R}^d$. Accordingly, at least $d+1$ UAVs in $\boldsymbol{r}$ must be selected as leaders to affinely span $\mathbb{R}^d$.

Let $\bar{\boldsymbol{\Omega}} = \boldsymbol{\Omega} \otimes \boldsymbol{I}_d$ and

$$\bar{\boldsymbol{\Omega}} = \begin{bmatrix} \bar{\boldsymbol{\Omega}}_{\mathrm{ll}} & \bar{\boldsymbol{\Omega}}_{\mathrm{lf}} \\ \bar{\boldsymbol{\Omega}}_{\mathrm{fl}} & \bar{\boldsymbol{\Omega}}_{\mathrm{ff}} \end{bmatrix}, \tag{4}$$

where $\bar{\boldsymbol{\Omega}}_{\mathrm{ll}} \in \mathbb{R}^{(dn_{\mathrm{l}})\times(dn_{\mathrm{l}})}$, $\bar{\boldsymbol{\Omega}}_{\mathrm{lf}} \in \mathbb{R}^{(dn_{\mathrm{l}})\times(dn_{\mathrm{f}})}$, $\bar{\boldsymbol{\Omega}}_{\mathrm{fl}} \in \mathbb{R}^{(dn_{\mathrm{f}})\times(dn_{\mathrm{l}})}$, and $\bar{\boldsymbol{\Omega}}_{\mathrm{ff}} \in \mathbb{R}^{(dn_{\mathrm{f}})\times(dn_{\mathrm{f}})}$. Obviously, $\bar{\boldsymbol{\Omega}}\boldsymbol{p} = \boldsymbol{0}$ is obtained from Eq. (1). Next, it is necessary to explain the relationship between affine localizability and the stress matrix.

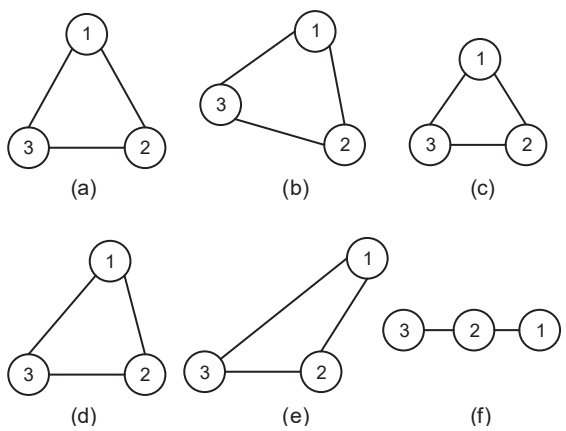

Fig. 1 An illustration of affine transformations of a nominal configuration: (a) nominal; (b) rotation; (c) scaling; (d−f) shear

Assumption 2 Assume that the nominal formation $(G,\ \boldsymbol{r})$ has a positive semidefinite stress matrix $\boldsymbol{\Omega}$ satisfying $\mathrm{rank}(\boldsymbol{\Omega}) = n-d-1$.

Lemma 2 (Zhao SY, 2018) Under Assumptions 1 and 2, the nominal formation $(G,\boldsymbol{r})$ is affinely localizable if and only if $\bar{\boldsymbol{\Omega}}_{\mathrm{ff}}$ is nonsingular. Accordingly, $\boldsymbol{p}_{\mathrm{f}}$ can be uniquely calculated as $\boldsymbol{p}_{\mathrm{f}} = -\bar{\boldsymbol{\Omega}}_{\mathrm{ff}}^{-1}\bar{\boldsymbol{\Omega}}_{\mathrm{fl}}\boldsymbol{p}_{\mathrm{l}}$ for any $\boldsymbol{p} = \left[\boldsymbol{p}_{\mathrm{l}}^{\mathrm{T}}, \boldsymbol{p}_{\mathrm{f}}^{\mathrm{T}}\right]^{\mathrm{T}} \in \mathcal{A}(\boldsymbol{r})$.

Assumption 3 Suppose that $(G,\boldsymbol{r})$ in $\mathbb{R}^d$ is affinely localizable by the leaders.

2.4 Problem formulation

Suppose that all n fixed-wing UAVs are flying at the same altitude and $d=2$. The kinematic equations of the ith fixed-wing UAV are described as

$$\begin{cases} \dot{x}_i = v_i\cos\theta_i, \\ \dot{y}_i = v_i\sin\theta_i, \\ \dot{\theta}_i = \omega_i, \end{cases} \tag{5}$$

where θ_i is the UAV's heading angle. The heading vector $\boldsymbol{h}_i = [\cos\theta_i, \sin\theta_i]^{\mathrm{T}}$ and its perpendicular vector $\boldsymbol{h}_i^{\perp} = [-\sin\theta_i, \cos\theta_i]^{\mathrm{T}}$ are introduced. Let $\boldsymbol{h}_{\mathrm{l}} = [\boldsymbol{h}_1^{\mathrm{T}}, \boldsymbol{h}_2^{\mathrm{T}}, \cdots, \boldsymbol{h}_{n_{\mathrm{l}}}^{\mathrm{T}}]^{\mathrm{T}} \in \mathbb{R}^{2n_{\mathrm{l}}}$, $\boldsymbol{h}_{\mathrm{f}} = [\boldsymbol{h}_{n_{\mathrm{l}}+1}^{\mathrm{T}}, \boldsymbol{h}_{n_{\mathrm{l}}+2}^{\mathrm{T}}, \cdots, \boldsymbol{h}_n^{\mathrm{T}}]^{\mathrm{T}} \in \mathbb{R}^{2n_{\mathrm{f}}}$, and $\boldsymbol{h} = [\boldsymbol{h}_{\mathrm{l}}^{\mathrm{T}}, \boldsymbol{h}_{\mathrm{f}}^{\mathrm{T}}]^{\mathrm{T}}$. The linear speed v_i and angular speed ω_i are the control inputs of the ith UAV, and are limited by the characteristics of fixed-wing UAVs:

$$0 < v_{\min} \le v_i \le v_{\max}, \quad |\,\omega_i\,| \le \omega_{\max}, \tag{6}$$

where $v_{\min}$ and $v_{\max}$ represent the minimum and maximum of the linear speed respectively, and $\omega_{\max}$ is the maximum angular speed.

Remark 1 In fact, Eq. (5) is widely used to study the formation control problem of multiple fixed-wing UAVs. The control of flight altitude is usually ignored in the cooperative control problem. In addition, Eq. (5) simplifies the actuator's dynamic characteristics. Consequently, the navigation control inputs, v_i and ω_i, need to be transformed to guide the bottom flight control of fixed-wing UAVs.

Let $\boldsymbol{v}_{\mathrm{l}} = [v_1, v_2, \cdots, v_{n_{\mathrm{l}}}]^{\mathrm{T}}$, $\boldsymbol{v}_{\mathrm{f}} = \left[v_{n_{\mathrm{l}}+1}, v_{n_{\mathrm{l}}+2}, \cdots, v_n\right]^{\mathrm{T}}$, and $\boldsymbol{v} = \left[\boldsymbol{v}_{\mathrm{l}}^{\mathrm{T}}, \boldsymbol{v}_{\mathrm{f}}^{\mathrm{T}}\right]^{\mathrm{T}} \in \mathbb{R}^n$. Similarly, $\boldsymbol{\omega} = \left[\boldsymbol{\omega}_{\mathrm{l}}^{\mathrm{T}}, \boldsymbol{\omega}_{\mathrm{f}}^{\mathrm{T}}\right]^{\mathrm{T}} = [\omega_1, \omega_2, \cdots, \omega_n]^{\mathrm{T}} \in \mathbb{R}^n$. Define

$$\boldsymbol{H} = \begin{bmatrix} \boldsymbol{h}_1 & & & & & \\ & \ddots & & & & \\ & & \boldsymbol{h}_{n_{\mathrm{l}}} & & & \\ & & & \boldsymbol{h}_{n_{\mathrm{l}}+1} & & \\ & & & & \ddots & \\ & & & & & \boldsymbol{h}_n \end{bmatrix} = \begin{bmatrix} \boldsymbol{H}_{\mathrm{l}} & \\ & \boldsymbol{H}_{\mathrm{f}} \end{bmatrix} \in \mathbb{R}^{2n\times n}.$$

Let $\boldsymbol{H}^{\perp} = \mathrm{diag}(\boldsymbol{h}_1^{\perp},\ \boldsymbol{h}_2^{\perp}, \cdots, \boldsymbol{h}_n^{\perp})$. Then the unicycle model (5) is rewritten as

$$\begin{cases} \dot{\boldsymbol{p}} &= \boldsymbol{H}\boldsymbol{v}, \\ \dot{\boldsymbol{h}} &= \boldsymbol{H}^{\perp}\boldsymbol{\omega}. \end{cases} \tag{7}$$

As shown in Eq. (3), the target formation of the multi-UAV system is defined. The control objective of the affine tracking problem is to drive all fixed-wing UAVs to converge to the desired states: $\lim\limits_{t\to\infty}\boldsymbol{p}(t) = \boldsymbol{p}^*(t)$ and $\lim\limits_{t\to\infty}\boldsymbol{h}(t) = \boldsymbol{h}^*(t)$. Assume that $v_i > 0$ and $\omega_i = \omega_{\mathrm{c}}$ for any $i \in \mathcal{V}_{\mathrm{l}}$, where ω_{c} is the homogeneous angular speed for leaders and $-\omega_{\max} < \omega_{\mathrm{c}} < \omega_{\max}$. Meanwhile, suppose that the leader information is known by the followers. When Assumptions 1−3 hold, if $\boldsymbol{p}_{\mathrm{l}}(t) = \boldsymbol{p}_{\mathrm{l}}^*(t)$ and $\boldsymbol{h}_{\mathrm{l}}(t) = \boldsymbol{h}_{\mathrm{l}}^*(t)$, then $\boldsymbol{p}_{\mathrm{f}}^* = -\bar{\boldsymbol{\Omega}}_{\mathrm{ff}}^{-1}\bar{\boldsymbol{\Omega}}_{\mathrm{fl}}\boldsymbol{p}_{\mathrm{l}}^*$. Define the formation tracking errors of followers as

$$\begin{aligned} \boldsymbol{\delta}_{\mathrm{p_f}}(t) =& \boldsymbol{p}_{\mathrm{f}}(t) - \boldsymbol{p}_{\mathrm{f}}^*(t) = \boldsymbol{p}_{\mathrm{f}}(t) + \bar{\boldsymbol{\Omega}}_{\mathrm{ff}}^{-1}\bar{\boldsymbol{\Omega}}_{\mathrm{fl}}\boldsymbol{p}_{\mathrm{l}}^*(t), \\ \boldsymbol{\delta}_{\mathrm{h_f}}(t) =& \boldsymbol{h}_{\mathrm{f}}(t) - \boldsymbol{h}_{\mathrm{f}}^*(t), \end{aligned} \tag{8}$$

where $\boldsymbol{\delta}_{\mathrm{p_f}}(t)$ represents the position error and $\boldsymbol{\delta}_{\mathrm{h_f}}(t)$ represents the heading error.

Problem 1 Given a team of n fixed-wing UAVs, each of which is modeled by Eq. (5), our objective is to design a control law $\boldsymbol{\mu} = [v_i, \omega_i]$ for each follower to track the time-varying target positions and to achieve affine transformations, i.e., $\lim\limits_{t\to\infty}\boldsymbol{\delta}_{\mathrm{p_f}}(t) = \boldsymbol{0}$ and $\lim\limits_{t\to\infty}\boldsymbol{\delta}_{\mathrm{h_f}}(t) = \boldsymbol{0}$.

3 Main results

In this section, we adopt the affine formation control scheme to solve Problem 1. Define $\tilde{\boldsymbol{v}}_{\mathrm{l}} = \mathrm{diag}(\boldsymbol{v}_{\mathrm{l}}) \otimes \boldsymbol{I}_2 \in \mathbb{R}^{2n_{\mathrm{l}}\times 2n_{\mathrm{l}}}$ and $\bar{\boldsymbol{v}}_{\mathrm{l}} = \tilde{\boldsymbol{v}}_{\mathrm{l}}\boldsymbol{h}_{\mathrm{l}} \in \mathbb{R}^{2n_{\mathrm{l}}}$.

Theorem 1 Under Assumptions 1−3, the control law designed for the ith follower is established

as

$$v_i = \boldsymbol{h}_i^{\mathrm{T}} \left[-\sum_{j\in\mathcal{N}_i} \varpi_{ij}(\boldsymbol{p}_i - \boldsymbol{p}_j) + \boldsymbol{k}_i \bar{\boldsymbol{v}}_{\mathrm{l}} + \omega_{\mathrm{c}} \boldsymbol{h}_i^{\perp} \right],$$
$$\omega_i = (\boldsymbol{h}_i^{\perp})^{\mathrm{T}} \left[-\sum_{j\in\mathcal{N}_i} \varpi_{ij}(\boldsymbol{p}_i - \boldsymbol{p}_j) + \boldsymbol{k}_i \bar{\boldsymbol{v}}_{\mathrm{l}} + \omega_{\mathrm{c}} \boldsymbol{h}_i^{\perp} \right], \tag{9}$$

where $\boldsymbol{k}_i \in \mathbb{R}^{2\times 2n_{\mathrm{l}}}$ is a matrix consisting the $2i-1$ and $2i$ rows of matrix $\boldsymbol{K} = -\bar{\boldsymbol{\Omega}}_{\mathrm{ff}}^{-1}\bar{\boldsymbol{\Omega}}_{\mathrm{fl}}$. As a result, the following results hold: the followers' tracking errors $\boldsymbol{\delta}_{\mathrm{p_f}}$ and $\boldsymbol{\delta}_{\mathrm{h_f}}$ can converge to zero when $v_i > 0$ for $i \in \mathcal{V}_{\mathrm{f}}$.

Proof Control law (9) can be rewritten as

$$\begin{aligned}\boldsymbol{v}_{\mathrm{f}} &= \boldsymbol{H}_{\mathrm{f}}^{\mathrm{T}} \left(-\bar{\boldsymbol{\Omega}}_{\mathrm{ff}}\boldsymbol{p}_{\mathrm{f}} - \bar{\boldsymbol{\Omega}}_{\mathrm{fl}}\boldsymbol{p}_{\mathrm{l}}^* - \bar{\boldsymbol{\Omega}}_{\mathrm{ff}}^{-1}\bar{\boldsymbol{\Omega}}_{\mathrm{fl}}\tilde{\boldsymbol{v}}_{\mathrm{l}}\boldsymbol{h}_{\mathrm{l}} + \omega_{\mathrm{c}}\boldsymbol{h}_{\mathrm{f}}^{\perp}\right),\\ \boldsymbol{\omega}_{\mathrm{f}} &= (\boldsymbol{H}_{\mathrm{f}}^{\perp})^{\mathrm{T}} \left(-\bar{\boldsymbol{\Omega}}_{\mathrm{ff}}\boldsymbol{p}_{\mathrm{f}} - \bar{\boldsymbol{\Omega}}_{\mathrm{fl}}\boldsymbol{p}_{\mathrm{l}}^* - \bar{\boldsymbol{\Omega}}_{\mathrm{ff}}^{-1}\bar{\boldsymbol{\Omega}}_{\mathrm{fl}}\tilde{\boldsymbol{v}}_{\mathrm{l}}\boldsymbol{h}_{\mathrm{l}} + \omega_{\mathrm{c}}\boldsymbol{h}_{\mathrm{f}}^{\perp}\right).\end{aligned} \tag{10}$$

Accordingly, the closed-loop dynamics is shown as

$$\begin{aligned}\dot{\boldsymbol{p}}_{\mathrm{f}} =& \boldsymbol{H}_{\mathrm{f}}\boldsymbol{H}_{\mathrm{f}}^{\mathrm{T}}\\ &\cdot\left(-\bar{\boldsymbol{\Omega}}_{\mathrm{ff}}\boldsymbol{p}_{\mathrm{f}} - \bar{\boldsymbol{\Omega}}_{\mathrm{fl}}\boldsymbol{p}_{\mathrm{l}}^* - \bar{\boldsymbol{\Omega}}_{\mathrm{ff}}^{-1}\bar{\boldsymbol{\Omega}}_{\mathrm{fl}}\tilde{\boldsymbol{v}}_{\mathrm{l}}\boldsymbol{h}_{\mathrm{l}} + \omega_{\mathrm{c}}\boldsymbol{h}_{\mathrm{f}}^{\perp}\right)\\ =& \boldsymbol{H}_{\mathrm{f}}\boldsymbol{H}_{\mathrm{f}}^{\mathrm{T}}\left(-\bar{\boldsymbol{\Omega}}_{\mathrm{ff}}\boldsymbol{p}_{\mathrm{f}} - \bar{\boldsymbol{\Omega}}_{\mathrm{fl}}\boldsymbol{p}_{\mathrm{l}}^* - \bar{\boldsymbol{\Omega}}_{\mathrm{ff}}^{-1}\bar{\boldsymbol{\Omega}}_{\mathrm{fl}}\tilde{\boldsymbol{v}}_{\mathrm{l}}\boldsymbol{h}_{\mathrm{l}}\right),\\ \dot{\boldsymbol{h}}_{\mathrm{f}} =& \boldsymbol{H}_{\mathrm{f}}^{\perp}(\boldsymbol{H}_{\mathrm{f}}^{\perp})^{\mathrm{T}}\\ &\cdot\left(-\bar{\boldsymbol{\Omega}}_{\mathrm{ff}}\boldsymbol{p}_{\mathrm{f}} - \bar{\boldsymbol{\Omega}}_{\mathrm{fl}}\boldsymbol{p}_{\mathrm{l}}^* - \bar{\boldsymbol{\Omega}}_{\mathrm{ff}}^{-1}\bar{\boldsymbol{\Omega}}_{\mathrm{fl}}\tilde{\boldsymbol{v}}_{\mathrm{l}}\boldsymbol{h}_{\mathrm{l}} + \omega_{\mathrm{c}}\boldsymbol{h}_{\mathrm{f}}^{\perp}\right)\\ =& \boldsymbol{H}_{\mathrm{f}}^{\perp}(\boldsymbol{H}_{\mathrm{f}}^{\perp})^{\mathrm{T}}\\ &\cdot\left(-\bar{\boldsymbol{\Omega}}_{\mathrm{ff}}\boldsymbol{p}_{\mathrm{f}} - \bar{\boldsymbol{\Omega}}_{\mathrm{fl}}\boldsymbol{p}_{\mathrm{l}}^* - \bar{\boldsymbol{\Omega}}_{\mathrm{ff}}^{-1}\bar{\boldsymbol{\Omega}}_{\mathrm{fl}}\tilde{\boldsymbol{v}}_{\mathrm{l}}\boldsymbol{h}_{\mathrm{l}}\right) + \omega_{\mathrm{c}}\boldsymbol{h}_{\mathrm{f}}^{\perp}.\end{aligned} \tag{11}$$

In Eq. (11), $-\bar{\boldsymbol{\Omega}}_{\mathrm{ff}}\boldsymbol{p}_{\mathrm{f}} - \bar{\boldsymbol{\Omega}}_{\mathrm{fl}}\boldsymbol{p}_{\mathrm{l}}^* = -\bar{\boldsymbol{\Omega}}_{\mathrm{ff}}\boldsymbol{p}_{\mathrm{f}} + \bar{\boldsymbol{\Omega}}_{\mathrm{ff}}\boldsymbol{p}_{\mathrm{f}}^* = -\bar{\boldsymbol{\Omega}}_{\mathrm{ff}}\boldsymbol{\delta}_{\mathrm{p_f}}$ is established because $\boldsymbol{p}_{\mathrm{f}}^* = -\bar{\boldsymbol{\Omega}}_{\mathrm{ff}}^{-1}\bar{\boldsymbol{\Omega}}_{\mathrm{fl}}\boldsymbol{p}_{\mathrm{l}}^*$ holds according to Lemma 2. Accordingly, the tracking error dynamics of Eq. (8) is

$$\begin{aligned}\dot{\boldsymbol{\delta}}_{\mathrm{p_f}} =& \dot{\boldsymbol{p}}_{\mathrm{f}} - \dot{\boldsymbol{p}}_{\mathrm{f}}^*\\ =& \boldsymbol{H}_{\mathrm{f}}\boldsymbol{H}_{\mathrm{f}}^{\mathrm{T}}\left(-\bar{\boldsymbol{\Omega}}_{\mathrm{ff}}\boldsymbol{p}_{\mathrm{f}} - \bar{\boldsymbol{\Omega}}_{\mathrm{fl}}\boldsymbol{p}_{\mathrm{l}}^* - \bar{\boldsymbol{\Omega}}_{\mathrm{ff}}^{-1}\bar{\boldsymbol{\Omega}}_{\mathrm{fl}}\tilde{\boldsymbol{v}}_{\mathrm{l}}\boldsymbol{h}_{\mathrm{l}}\right)\\ &+ \bar{\boldsymbol{\Omega}}_{\mathrm{ff}}^{-1}\bar{\boldsymbol{\Omega}}_{\mathrm{fl}}\dot{\boldsymbol{p}}_{\mathrm{l}}^*\\ =& -\boldsymbol{H}_{\mathrm{f}}\boldsymbol{H}_{\mathrm{f}}^{\mathrm{T}}\bar{\boldsymbol{\Omega}}_{\mathrm{ff}}\boldsymbol{\delta}_{\mathrm{p_f}} + \boldsymbol{H}_{\mathrm{f}}^{\perp}(\boldsymbol{H}_{\mathrm{f}}^{\perp})^{\mathrm{T}}\bar{\boldsymbol{\Omega}}_{\mathrm{ff}}^{-1}\bar{\boldsymbol{\Omega}}_{\mathrm{fl}}\tilde{\boldsymbol{v}}_{\mathrm{l}}\boldsymbol{h}_{\mathrm{l}},\\ \dot{\boldsymbol{\delta}}_{\mathrm{h_f}} =& \dot{\boldsymbol{h}}_{\mathrm{f}} - \dot{\boldsymbol{h}}_{\mathrm{f}}^*\\ =& \boldsymbol{H}_{\mathrm{f}}^{\perp}(\boldsymbol{H}_{\mathrm{f}}^{\perp})^{\mathrm{T}}\left(-\bar{\boldsymbol{\Omega}}_{\mathrm{ff}}\boldsymbol{p}_{\mathrm{f}} - \bar{\boldsymbol{\Omega}}_{\mathrm{fl}}\boldsymbol{p}_{\mathrm{l}}^* - \bar{\boldsymbol{\Omega}}_{\mathrm{ff}}^{-1}\bar{\boldsymbol{\Omega}}_{\mathrm{fl}}\tilde{\boldsymbol{v}}_{\mathrm{l}}\boldsymbol{h}_{\mathrm{l}}\right)\\ &+ \omega_{\mathrm{c}}\boldsymbol{h}_{\mathrm{f}}^{\perp} - \omega_{\mathrm{c}}(\boldsymbol{h}_{\mathrm{f}}^{\perp})^*\\ =& \boldsymbol{H}_{\mathrm{f}}^{\perp}(\boldsymbol{H}_{\mathrm{f}}^{\perp})^{\mathrm{T}}\left(-\bar{\boldsymbol{\Omega}}_{\mathrm{ff}}\boldsymbol{\delta}_{\mathrm{p_f}} - \bar{\boldsymbol{\Omega}}_{\mathrm{ff}}^{-1}\bar{\boldsymbol{\Omega}}_{\mathrm{fl}}\tilde{\boldsymbol{v}}_{\mathrm{l}}\boldsymbol{h}_{\mathrm{l}}\right)\\ &+ \omega_{\mathrm{c}}\left(\boldsymbol{h}_{\mathrm{f}}^{\perp} - (\boldsymbol{h}_{\mathrm{f}}^{\perp})^*\right).\end{aligned} \tag{12}$$

Let $\tilde{\boldsymbol{v}}_{\mathrm{f}}^* = \mathrm{diag}(v_{n_{\mathrm{l}}+1}^*, \cdots, v_i^*, \cdots, v_n^*)\otimes\boldsymbol{I}_2$, where v_i^* $(i \in \mathcal{V}_{\mathrm{f}})$ is the target linear speed of the ith follower. It is clear that $v_i^* > 0$ $(i \in \mathcal{V}_{\mathrm{f}})$ because the followers are driven to track the leaders and $v_q > 0$ for any $q \in \mathcal{V}_{\mathrm{l}}$. Therefore, all eigenvalues of diagonal matrix $\tilde{\boldsymbol{v}}_{\mathrm{f}}^*$ are positive and $\tilde{\boldsymbol{v}}_{\mathrm{f}}^*$ is positive definite. Meanwhile, $\tilde{\boldsymbol{v}}_{\mathrm{f}}^*\boldsymbol{h}_{\mathrm{f}}^* = -\bar{\boldsymbol{\Omega}}_{\mathrm{ff}}^{-1}\bar{\boldsymbol{\Omega}}_{\mathrm{fl}}\tilde{\boldsymbol{v}}_{\mathrm{l}}^*\boldsymbol{h}_{\mathrm{l}}^* = -\bar{\boldsymbol{\Omega}}_{\mathrm{ff}}^{-1}\bar{\boldsymbol{\Omega}}_{\mathrm{fl}}\tilde{\boldsymbol{v}}_{\mathrm{l}}\boldsymbol{h}_{\mathrm{l}}$ is obtained from the derivative of $\boldsymbol{p}_{\mathrm{f}}^* = -\bar{\boldsymbol{\Omega}}_{\mathrm{ff}}^{-1}\bar{\boldsymbol{\Omega}}_{\mathrm{fl}}\boldsymbol{p}_{\mathrm{l}}^*$.

We now prove the convergence of the proposed control law (9). Consider a Lyapunov function denoted as

$$V = \frac{1}{2}\boldsymbol{\delta}_{\mathrm{p_f}}^{\mathrm{T}}\bar{\boldsymbol{\Omega}}_{\mathrm{ff}}\boldsymbol{\delta}_{\mathrm{p_f}} + \frac{1}{2}\boldsymbol{\delta}_{\mathrm{h_f}}^{\mathrm{T}}\tilde{\boldsymbol{v}}_{\mathrm{f}}^*\boldsymbol{\delta}_{\mathrm{h_f}} \geq 0. \tag{13}$$

Combined with Eq. (12) , the derivative of V at time t is

$$\begin{aligned}\dot{V} =& \boldsymbol{\delta}_{\mathrm{p_f}}^{\mathrm{T}}\bar{\boldsymbol{\Omega}}_{\mathrm{ff}}\dot{\boldsymbol{\delta}}_{\mathrm{p_f}} + \boldsymbol{\delta}_{\mathrm{h_f}}^{\mathrm{T}}\tilde{\boldsymbol{v}}_{\mathrm{f}}^*\dot{\boldsymbol{\delta}}_{\mathrm{h_f}}\\ =& \boldsymbol{\delta}_{\mathrm{h_f}}^{\mathrm{T}}\tilde{\boldsymbol{v}}_{\mathrm{f}}^*\Big[\boldsymbol{H}_{\mathrm{f}}^{\perp}(\boldsymbol{H}_{\mathrm{f}}^{\perp})^{\mathrm{T}}\left(-\bar{\boldsymbol{\Omega}}_{\mathrm{ff}}\boldsymbol{\delta}_{\mathrm{p_f}} - \bar{\boldsymbol{\Omega}}_{\mathrm{ff}}^{-1}\bar{\boldsymbol{\Omega}}_{\mathrm{fl}}\tilde{\boldsymbol{v}}_{\mathrm{l}}\boldsymbol{h}_{\mathrm{l}}\right)\\ &+ \omega_{\mathrm{c}}\left(\boldsymbol{h}_{\mathrm{f}}^{\perp} - (\boldsymbol{h}_{\mathrm{f}}^{\perp})^*\right)\Big] - \boldsymbol{\delta}_{\mathrm{p_f}}^{\mathrm{T}}\bar{\boldsymbol{\Omega}}_{\mathrm{ff}}\boldsymbol{H}_{\mathrm{f}}\boldsymbol{H}_{\mathrm{f}}^{\mathrm{T}}\bar{\boldsymbol{\Omega}}_{\mathrm{ff}}\boldsymbol{\delta}_{\mathrm{p_f}}\\ &+ \boldsymbol{\delta}_{\mathrm{p_f}}^{\mathrm{T}}\bar{\boldsymbol{\Omega}}_{\mathrm{ff}}\boldsymbol{H}_{\mathrm{f}}^{\perp}(\boldsymbol{H}_{\mathrm{f}}^{\perp})^{\mathrm{T}}\bar{\boldsymbol{\Omega}}_{\mathrm{ff}}^{-1}\bar{\boldsymbol{\Omega}}_{\mathrm{fl}}\tilde{\boldsymbol{v}}_{\mathrm{l}}\boldsymbol{h}_{\mathrm{l}}\\ =& -\boldsymbol{\delta}_{\mathrm{p_f}}^{\mathrm{T}}\bar{\boldsymbol{\Omega}}_{\mathrm{ff}}\boldsymbol{H}_{\mathrm{f}}\boldsymbol{H}_{\mathrm{f}}^{\mathrm{T}}\bar{\boldsymbol{\Omega}}_{\mathrm{ff}}\boldsymbol{\delta}_{\mathrm{p_f}}\\ &+ \boldsymbol{\delta}_{\mathrm{p_f}}^{\mathrm{T}}\bar{\boldsymbol{\Omega}}_{\mathrm{ff}}\boldsymbol{H}_{\mathrm{f}}^{\perp}(\boldsymbol{H}_{\mathrm{f}}^{\perp})^{\mathrm{T}}\bar{\boldsymbol{\Omega}}_{\mathrm{ff}}^{-1}\bar{\boldsymbol{\Omega}}_{\mathrm{fl}}\tilde{\boldsymbol{v}}_{\mathrm{l}}\boldsymbol{h}_{\mathrm{l}}\\ &-(\boldsymbol{h}_{\mathrm{f}} - \boldsymbol{h}_{\mathrm{f}}^*)^{\mathrm{T}}\tilde{\boldsymbol{v}}_{\mathrm{f}}^*\boldsymbol{H}_{\mathrm{f}}^{\perp}(\boldsymbol{H}_{\mathrm{f}}^{\perp})^{\mathrm{T}}\bar{\boldsymbol{\Omega}}_{\mathrm{ff}}\boldsymbol{\delta}_{\mathrm{p_f}}\\ &- (\boldsymbol{h}_{\mathrm{f}} - \boldsymbol{h}_{\mathrm{f}}^*)^{\mathrm{T}}\tilde{\boldsymbol{v}}_{\mathrm{f}}^*\boldsymbol{H}_{\mathrm{f}}^{\perp}(\boldsymbol{H}_{\mathrm{f}}^{\perp})^{\mathrm{T}}\bar{\boldsymbol{\Omega}}_{\mathrm{ff}}^{-1}\bar{\boldsymbol{\Omega}}_{\mathrm{fl}}\tilde{\boldsymbol{v}}_{\mathrm{l}}\boldsymbol{h}_{\mathrm{l}}\\ &+ \omega_{\mathrm{c}}(\boldsymbol{h}_{\mathrm{f}} - \boldsymbol{h}_{\mathrm{f}}^*)^{\mathrm{T}}\tilde{\boldsymbol{v}}_{\mathrm{f}}^*\left(\boldsymbol{h}_{\mathrm{f}}^{\perp} - (\boldsymbol{h}_{\mathrm{f}}^{\perp})^*\right)\\ =& -\boldsymbol{\delta}_{\mathrm{p_f}}^{\mathrm{T}}\bar{\boldsymbol{\Omega}}_{\mathrm{ff}}\boldsymbol{H}_{\mathrm{f}}\boldsymbol{H}_{\mathrm{f}}^{\mathrm{T}}\bar{\boldsymbol{\Omega}}_{\mathrm{ff}}\boldsymbol{\delta}_{\mathrm{p_f}} + \boldsymbol{\delta}_{\mathrm{p_f}}^{\mathrm{T}}\bar{\boldsymbol{\Omega}}_{\mathrm{ff}}\boldsymbol{H}_{\mathrm{f}}^{\perp}(\boldsymbol{H}_{\mathrm{f}}^{\perp})^{\mathrm{T}}\\ &\cdot\bar{\boldsymbol{\Omega}}_{\mathrm{ff}}^{-1}\bar{\boldsymbol{\Omega}}_{\mathrm{fl}}\tilde{\boldsymbol{v}}_{\mathrm{l}}\boldsymbol{h}_{\mathrm{l}} + \boldsymbol{h}_{\mathrm{l}}^{\mathrm{T}}\tilde{\boldsymbol{v}}_{\mathrm{l}}\bar{\boldsymbol{\Omega}}_{\mathrm{fl}}^{\mathrm{T}}\bar{\boldsymbol{\Omega}}_{\mathrm{ff}}^{-1}\boldsymbol{H}_{\mathrm{f}}^{\perp}(\boldsymbol{H}_{\mathrm{f}}^{\perp})^{\mathrm{T}}\\ &\cdot\left(-\bar{\boldsymbol{\Omega}}_{\mathrm{ff}}\boldsymbol{\delta}_{\mathrm{p_f}} - \bar{\boldsymbol{\Omega}}_{\mathrm{ff}}^{-1}\bar{\boldsymbol{\Omega}}_{\mathrm{fl}}\tilde{\boldsymbol{v}}_{\mathrm{l}}\boldsymbol{h}_{\mathrm{l}}\right)\\ =& -\boldsymbol{\delta}_{\mathrm{p_f}}^{\mathrm{T}}\bar{\boldsymbol{\Omega}}_{\mathrm{ff}}\boldsymbol{H}_{\mathrm{f}}\boldsymbol{H}_{\mathrm{f}}^{\mathrm{T}}\bar{\boldsymbol{\Omega}}_{\mathrm{ff}}\boldsymbol{\delta}_{\mathrm{p_f}}\\ &- (\boldsymbol{h}_{\mathrm{f}}^*)^{\mathrm{T}}(\tilde{\boldsymbol{v}}_{\mathrm{f}}^*)^{\mathrm{T}}\boldsymbol{H}_{\mathrm{f}}^{\perp}(\boldsymbol{H}_{\mathrm{f}}^{\perp})^{\mathrm{T}}\tilde{\boldsymbol{v}}_{\mathrm{f}}^*\boldsymbol{h}_{\mathrm{f}}^*\\ =& -\|\boldsymbol{\delta}_{\mathrm{p_f}}^{\mathrm{T}}\bar{\boldsymbol{\Omega}}_{\mathrm{ff}}\boldsymbol{H}_{\mathrm{f}}\|^2 - \|(\boldsymbol{H}_{\mathrm{f}}^{\perp})^{\mathrm{T}}\tilde{\boldsymbol{v}}_{\mathrm{f}}^*\boldsymbol{h}_{\mathrm{f}}^*\|^2\\ \leq& 0.\end{aligned} \tag{14}$$

First of all, let us analyze the heading error $\boldsymbol{\delta}_{\mathrm{h_f}}$. If $\lim_{t\to\infty}\dot{V} = 0$ holds, $(\boldsymbol{H}_{\mathrm{f}}^{\perp})^{\mathrm{T}}\tilde{\boldsymbol{v}}_{\mathrm{f}}^*\boldsymbol{h}_{\mathrm{f}}^* = \boldsymbol{0}$ is obtained, which means $(\boldsymbol{h}_{\mathrm{f}}^{\perp})^{\mathrm{T}}\boldsymbol{h}_{\mathrm{f}}^* = \boldsymbol{0}$. Thus, it is obvious to deduce $\boldsymbol{h}_{\mathrm{f}} = \boldsymbol{h}_{\mathrm{f}}^*$ or $\boldsymbol{h}_{\mathrm{f}} = -\boldsymbol{h}_{\mathrm{f}}^*$. According to Eq. (12), if $\dot{V} = 0$, $\dot{\boldsymbol{\delta}}_{\mathrm{p_f}} = -\boldsymbol{H}_{\mathrm{f}}\boldsymbol{H}_{\mathrm{f}}^{\mathrm{T}}\bar{\boldsymbol{\Omega}}_{\mathrm{ff}}\boldsymbol{\delta}_{\mathrm{p_f}} + \boldsymbol{H}_{\mathrm{f}}^{\perp}(\boldsymbol{H}_{\mathrm{f}}^{\perp})^{\mathrm{T}}\bar{\boldsymbol{\Omega}}_{\mathrm{ff}}^{-1}\bar{\boldsymbol{\Omega}}_{\mathrm{fl}}\tilde{\boldsymbol{v}}_{\mathrm{l}}\boldsymbol{h}_{\mathrm{l}} = -\boldsymbol{H}_{\mathrm{f}}\boldsymbol{H}_{\mathrm{f}}^{\mathrm{T}}\bar{\boldsymbol{\Omega}}_{\mathrm{ff}}\boldsymbol{\delta}_{\mathrm{p_f}} - \boldsymbol{H}_{\mathrm{f}}^{\perp}(\boldsymbol{H}_{\mathrm{f}}^{\perp})^{\mathrm{T}}\tilde{\boldsymbol{v}}_{\mathrm{f}}^*\boldsymbol{h}_{\mathrm{f}}^* = \boldsymbol{0}$ is obtained. Thus, $\tilde{\boldsymbol{v}}_{\mathrm{f}}\boldsymbol{h}_{\mathrm{f}} = \tilde{\boldsymbol{v}}_{\mathrm{f}}^*\boldsymbol{h}_{\mathrm{f}}^*$ holds because $\dot{\boldsymbol{p}}_{\mathrm{f}} = \dot{\boldsymbol{p}}_{\mathrm{f}}^*(t)$. When $\boldsymbol{h}_{\mathrm{f}} = -\boldsymbol{h}_{\mathrm{f}}^*$ holds, $\tilde{\boldsymbol{v}}_{\mathrm{f}} = -\tilde{\boldsymbol{v}}_{\mathrm{f}}^*$ is obtained, which contradicts $v_i > 0$, $\forall\, i \in \mathcal{V}_{\mathrm{f}}$. Correspondingly, $\boldsymbol{h}_{\mathrm{f}} = \boldsymbol{h}_{\mathrm{f}}^*$ is reasonable, and $\boldsymbol{\delta}_{\mathrm{h_f}} = \boldsymbol{h}_{\mathrm{f}}(t) - \boldsymbol{h}_{\mathrm{f}}^*(t) = \boldsymbol{0}$ holds.

Second, consider the convergence of $\boldsymbol{\delta}_{\mathrm{p_f}}$. $\boldsymbol{\delta}_{\mathrm{p_f}}^{\mathrm{T}}\bar{\boldsymbol{\Omega}}_{\mathrm{ff}}\boldsymbol{H}_{\mathrm{f}} = \boldsymbol{0}$ is obtained from $\lim_{t\to\infty}\dot{V} = 0$.

According to LaSalle's invariance principle, the tracking error $\boldsymbol{\delta}_{\mathrm{pf}}$ would converge to $\{\boldsymbol{\delta}_{\mathrm{pf}}|\boldsymbol{\delta}_{\mathrm{pf}}^{\mathrm{T}}\bar{\boldsymbol{\Omega}}_{\mathrm{ff}}\boldsymbol{H}_{\mathrm{f}}=\mathbf{0}\}$. There are two conditions:

(1) $\boldsymbol{\delta}_{\mathrm{pf}}^{\mathrm{T}}\bar{\boldsymbol{\Omega}}_{\mathrm{ff}}=\mathbf{0}$. Because $\bar{\boldsymbol{\Omega}}_{\mathrm{ff}}$ is positive definite, $\boldsymbol{\delta}_{\mathrm{pf}}=\mathbf{0}$ is obtained under this condition. Therefore, the target affine formation can be achieved.

(2) $\boldsymbol{\delta}_{\mathrm{pf}}^{\mathrm{T}}\bar{\boldsymbol{\Omega}}_{\mathrm{ff}}\neq\mathbf{0}$ and $\boldsymbol{\delta}_{\mathrm{pf}}^{\mathrm{T}}\bar{\boldsymbol{\Omega}}_{\mathrm{ff}}\boldsymbol{H}_{\mathrm{f}}=\mathbf{0}$. It has been proved that when $v_i>0$ for $i\in\mathcal{V}_{\mathrm{f}}$, $\boldsymbol{\delta}_{\mathrm{hf}}=\mathbf{0}$ and $\boldsymbol{h}_{\mathrm{f}}=\boldsymbol{h}_{\mathrm{f}}^{*}$ hold when $t\to\infty$. Therefore, $\dot{\boldsymbol{\delta}}_{\mathrm{hf}}=\dot{\boldsymbol{h}}_{\mathrm{f}}-\dot{\boldsymbol{h}}_{\mathrm{f}}^{*}=\mathbf{0}$ is established. According to Eq. (12), we have

$$\begin{aligned}\dot{\boldsymbol{\delta}}_{\mathrm{hf}}=&\boldsymbol{H}_{\mathrm{f}}^{\perp}(\boldsymbol{H}_{\mathrm{f}}^{\perp})^{\mathrm{T}}\left(-\bar{\boldsymbol{\Omega}}_{\mathrm{ff}}\boldsymbol{\delta}_{\mathrm{pf}}+\tilde{\boldsymbol{v}}_{\mathrm{f}}^{*}\boldsymbol{h}_{\mathrm{f}}^{*}\right)\\&+\omega_{\mathrm{c}}\left(\boldsymbol{h}_{\mathrm{f}}^{\perp}-(\boldsymbol{h}_{\mathrm{f}}^{\perp})^{*}\right)\\=&-\left(\boldsymbol{H}_{\mathrm{f}}\boldsymbol{H}_{\mathrm{f}}^{\mathrm{T}}-\boldsymbol{I}\right)\bar{\boldsymbol{\Omega}}_{\mathrm{ff}}\boldsymbol{\delta}_{\mathrm{pf}}+\boldsymbol{H}_{\mathrm{f}}^{\perp}(\boldsymbol{H}_{\mathrm{f}}^{\perp})^{\mathrm{T}}\tilde{\boldsymbol{v}}_{\mathrm{f}}^{*}\boldsymbol{h}_{\mathrm{f}}^{*}\\=&-\boldsymbol{H}_{\mathrm{f}}\boldsymbol{H}_{\mathrm{f}}^{\mathrm{T}}\bar{\boldsymbol{\Omega}}_{\mathrm{ff}}\boldsymbol{\delta}_{\mathrm{pf}}+\bar{\boldsymbol{\Omega}}_{\mathrm{ff}}\boldsymbol{\delta}_{\mathrm{pf}}+\boldsymbol{H}_{\mathrm{f}}^{\perp}(\boldsymbol{H}_{\mathrm{f}}^{\perp})^{\mathrm{T}}\tilde{\boldsymbol{v}}_{\mathrm{f}}^{*}\boldsymbol{h}_{\mathrm{f}}^{*}\\=&\bar{\boldsymbol{\Omega}}_{\mathrm{ff}}\boldsymbol{\delta}_{\mathrm{pf}}\\\neq&\mathbf{0},\end{aligned}$$

which contradicts $\dot{\boldsymbol{\delta}}_{\mathrm{hf}}=\mathbf{0}$. Consequently, this condition does not exist.

In conclusion, $\boldsymbol{\delta}_{\mathrm{pf}}$ and $\boldsymbol{\delta}_{\mathrm{hf}}$ would converge to zero provided that $v_i>0$, $\forall\, i\in\mathcal{V}_{\mathrm{f}}$.

Remark 2 Control law (9) consists of two parts: affine formation generation and velocity matching. The first term in the brackets [ ] in Eq. (9) is the consensus protocol of positions, and the last two terms aim at achieving velocity matching among the leaders and followers. Therefore, the system with multiple fixed-wing UAVs can track different trajectories and achieve any time-varying affine transformations. As a result, the maneuverability in dynamic environments is improved.

In fact, the speeds of fixed-wing UAVs are bounded, as described in inequality (6). The linear speeds during flight must be positive so that $v_i>0$ for $i\in\mathcal{V}_{\mathrm{f}}$ is an achievable requirement. To meet the speed constraints in inequality (6), a saturated control strategy is proposed as follows:

Define a saturation function $\mathrm{sat}(x,a,b)$ to limit the input values. Supposing $a<b$, the saturation function is defined as

$$\mathrm{sat}(x,a,b)=\begin{cases}a, & x<a,\\ x, & a\leq x\leq b,\\ b, & x>b.\end{cases}\tag{15}$$

Therefore, the proposed affine formation control law (9) can be modified as

$$\begin{aligned}v_i=&\mathrm{sat}\Bigg(\boldsymbol{h}_i^{\mathrm{T}}\Bigg(-\sum_{j\in\mathcal{N}_i}\varpi_{ij}(\boldsymbol{p}_i-\boldsymbol{p}_j)+\boldsymbol{k}_i\bar{\boldsymbol{v}}_{\mathrm{l}}+\omega_{\mathrm{c}}\boldsymbol{h}_i^{\perp}\Bigg),\\&v_{\min},v_{\max}\Bigg),\\\omega_i=&\mathrm{sat}\Bigg(\boldsymbol{h}_i^{\perp\mathrm{T}}\Bigg(-\sum_{j\in\mathcal{N}_i}\varpi_{ij}(\boldsymbol{p}_i-\boldsymbol{p}_j)+\boldsymbol{k}_i\bar{\boldsymbol{v}}_{\mathrm{l}}+\omega_{\mathrm{c}}\boldsymbol{h}_i^{\perp}\Bigg),\\&-\omega_{\max},\omega_{\max}\Bigg).\end{aligned}\tag{16}$$

Simulation results presented in Section 4 verify that the saturated control strategy is effective in constraining the control inputs, and that the tracking errors would like to converge to zero under control law (16). In other words, fixed-wing UAVs can achieve target affine formation while tracking different trajectories without breaking the speed constraints.

Remark 3 The modified control law (16) is closely related to the physical characteristics of fixed-wing UAVs. It is meaningful but challenging to analyze the convergence of the nonlinear system with asymmetrical input constraints. The proposed saturated control strategy is a simple and practical method to limit the value range of speeds, which is inspired by Fathian et al. (2018) and Zhao SY (2018). Next, further stability analysis of the nonlinear system with speed constraints is carried out.

4 Simulations

In this section, we present simulation examples of six fixed-wing UAVs to verify the effectiveness of the proposed affine formation tracking control law (16). The nominal formation $(G,\boldsymbol{r})$ is given in Fig. 2. In a 2D space, the first three UAVs are chosen as the leaders and the other three UAVs are the followers. The nominal configuration is set as $\boldsymbol{r}_{\mathrm{l}}=8\left[\sqrt{3},0,0,1,0,-1\right]^{\mathrm{T}}$ and $\boldsymbol{r}_{\mathrm{f}}=8\left[-\sqrt{3},2,-\sqrt{3},0,-\sqrt{3},-2\right]^{\mathrm{T}}$. Accordingly, the stress matrix is calculated using the algorithm proposed in Zhao SY (2018), and the weights are labeled at the corresponding edges in Fig. 2. The speed constraints are set as $v_{\min}=10$ m/s, $v_{\max}=25$ m/s, and $\omega_{\max}=0.5$ rad/s.

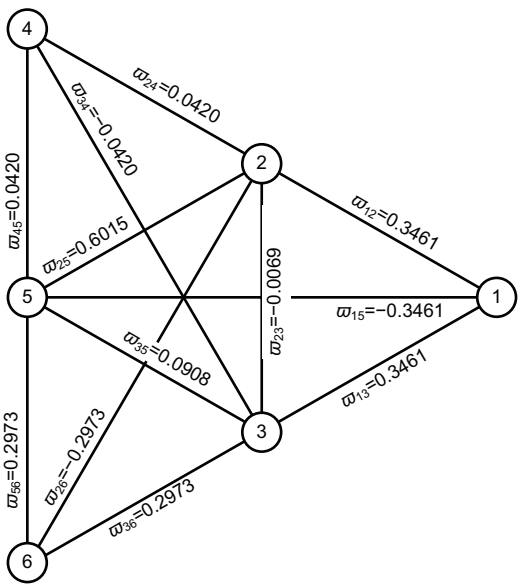

Fig. 2 Nominal formation of six fixed-wing UAVs

4.1 Trajectory tracking

The first simulation example shown in Fig. 3 demonstrates that control law (16) can track different trajectories in a 2D space. In Fig. 3a, leaders move in a straight line and the heading angles are the same, i.e., $\omega_c = 0$. Let $v_i = 15$ m/s for all $i \in \mathcal{V}_l$. The initial states of the leaders are $[\boldsymbol{p}_1; \theta_1] = [16\sqrt{3}, 0, \frac{1}{6}\pi]^{\mathrm{T}}$, $[\boldsymbol{p}_2; \theta_2] = [0, 16\sqrt{3}, \frac{1}{6}\pi]^{\mathrm{T}}$, and $[\boldsymbol{p}_3; \theta_3] = [0, -16\sqrt{3}, \frac{1}{6}\pi]^{\mathrm{T}}$, which means that the leaders' configuration has a larger size than the nominal configuration. Set the initial states of the followers arbitrarily. As shown in Fig. 3a, the followers finally converge to their desired states. Also, the distance error $\boldsymbol{\delta}_{\mathrm{pf}}$ shown in Fig. 4a indicates that the target formation is generated. Fig. 5a shows that the saturation function can prevent the linear and angular speeds from exceeding the upper or lower bounds of the speeds specified in inequality (6).

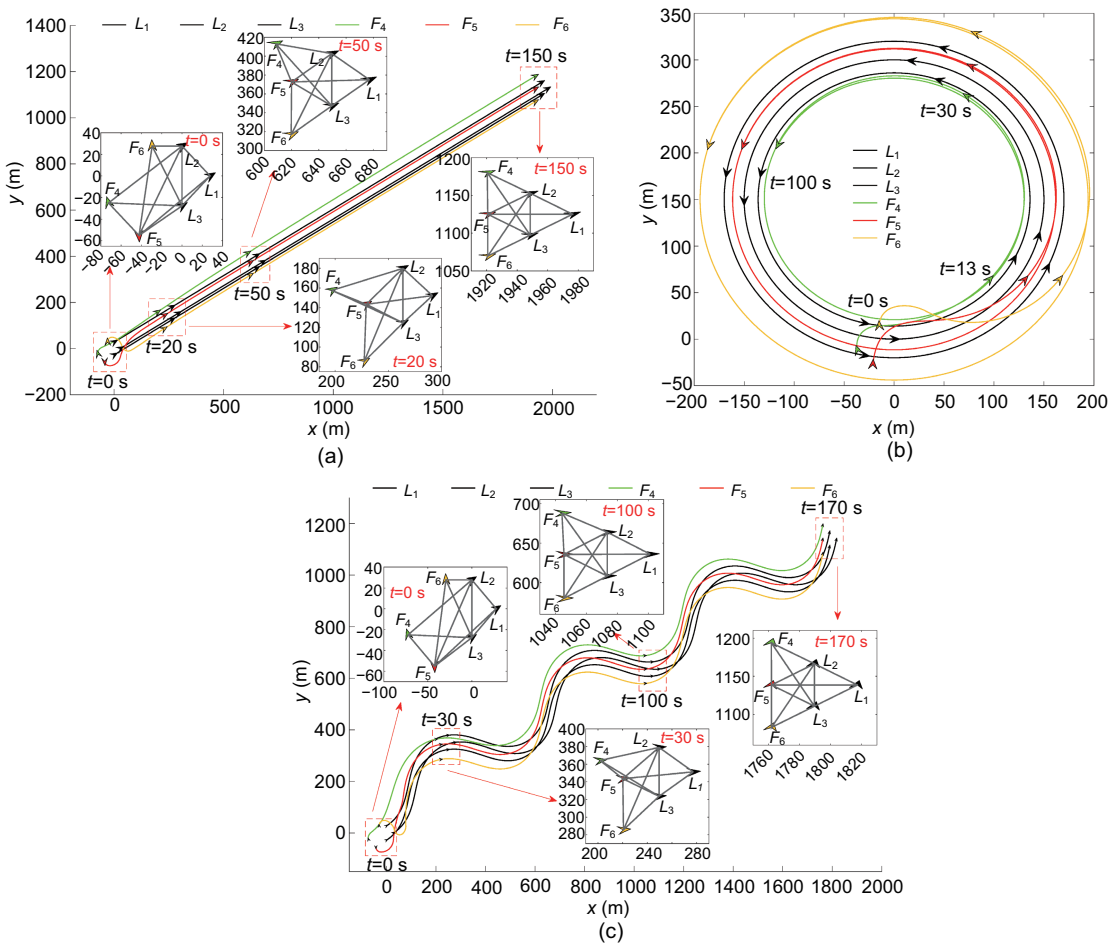

Fig. 3 A simulation example to illustrate the affine formation tracking control law (16). The leaders move along different trajectories: (a) straight line; (b) circle; (c) sine curve (L: leader; F: follower)

In Fig. 3b, leaders move in a circle, and $\omega_c = 0.1$ rad/s is set to declare the rotation of the nominal formation. The initial states of the leaders are $[\boldsymbol{p}_1;\theta_1] = [0,0,0]^{\mathrm{T}}$, $[\boldsymbol{p}_2;\theta_2] = [-30,10\sqrt{3},-0.2225]^{\mathrm{T}}$, and $[\boldsymbol{p}_3;\theta_3] = [-30,-10\sqrt{3},-0.1777]^{\mathrm{T}}$. Because the initial positions of the leaders are not in the nominal configuration, the scale of the target formation is different from the nominal formation. To keep the target configuration, the leaders move along different circular trajectories so that their linear speeds are not the same. Accordingly, the linear speeds of the followers cannot converge to the same constant, but the angular speeds are homogeneous, as shown in Fig. 5b. Trajectories of the six UAVs are described in Fig. 3b. It can be clearly seen that the six UAVs can form target formation and realize rotation. The distance errors in Fig. 4b converge to zero, which illustrates the generation of target formation and affine transformation. In Fig. 3c, the speeds of leaders are set as $v_i = 15 - \cos(0.12t)$ m/s and $\omega_i = 0.1\cos(0.12t)$ rad/s for all $i \in \mathcal{V}_l$, which are time-varying and reasonable in reality. It is clear that the formation tracking error $\boldsymbol{\delta}_{\mathrm{pf}}$ converges to zero (Fig. 4c), and that the linear speed v_i and angular speed ω_i are bounded (Fig. 5c).

In the simulation, the speeds and trajectories of the three leaders are generated in advance. The results demonstrate that the saturated affine formation tracking control law (16) can drive UAVs to converge to the target states and to adapt to diverse trajectories, which is helpful in tracking the real-time trajectories generated from the tasks in practical applications.

To make the results more comparable, two different control laws proposed in Zhao SY (2018) and Xu et al. (2020) are applied to the formation tracking problem, where the leaders have the same speeds as shown in Fig. 3c. Fig. 6 exhibits the simulation results of the control law proposed in Zhao SY (2018), and Fig. 7 shows the simulation results of the method proposed in Xu et al. (2020). Obviously, tracking errors of the three followers cannot converge to zero and the control objectives are unachievable, proving

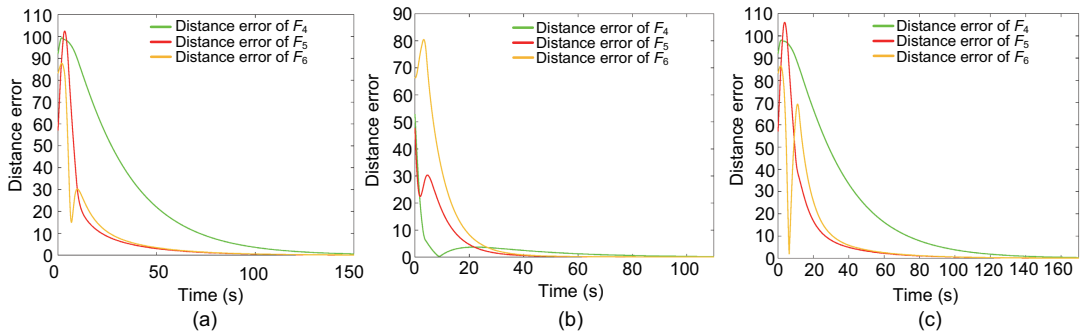

Fig. 4 Tracking errors of the three following fixed-wing UAVs in the affine formation. The leaders move along different trajectories: (a) straight line; (b) circle; (c) sine curve (F: follower)

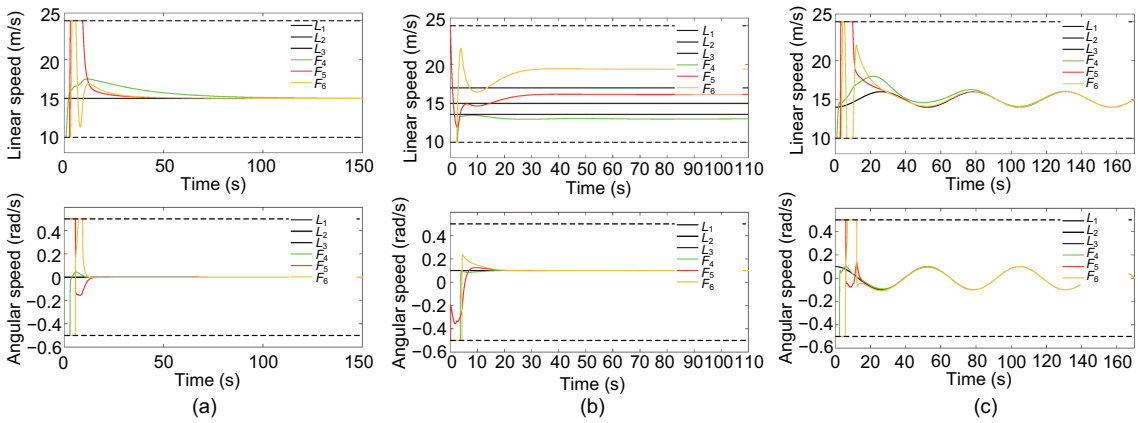

Fig. 5 Constrained linear and angular speeds of the fixed-wing UAVs in the affine formation. The leaders move along different trajectories: (a) straight line; (b) circle; (c) sine curve (L: leader; F: follower)

that the proposed control law in this study has a higher adaptability.

4.2 Affine transformations

The second simulation example demonstrates that the control law (16) can achieve affine transformations when the multi-UAV system maneuvers, as shown in Fig. 8. As can be seen in Fig. 9, the formation keeps maneuvering while changing its configuration, including the centroid, orientation, scale, and geometric pattern. In Fig. 10, the tracking error remains zero when the formation transforms its configuration affinely, except for two clockwise turnings from t=220 s and 290 s, because the configuration of the three leaders is not affinely transformed from the nominal configuration in those two moments. It is observed that the tracking error appears but converges to zero quickly. Accordingly, the affine formation tracking control law (16) shows favorable maneuverability, which can realize affine transformation of the fixed-wing UAV formation without breaking speed constraints.

5 Conclusions

To improve the maneuverability of fixed-wing UAV formations, the unicycle model with asymmetrical input constraints was applied to study the affine formation tracking control problem in this paper. Under the affine formation control scheme, the target formations were obtained from the affine transformations of the defined nominal formation, and the

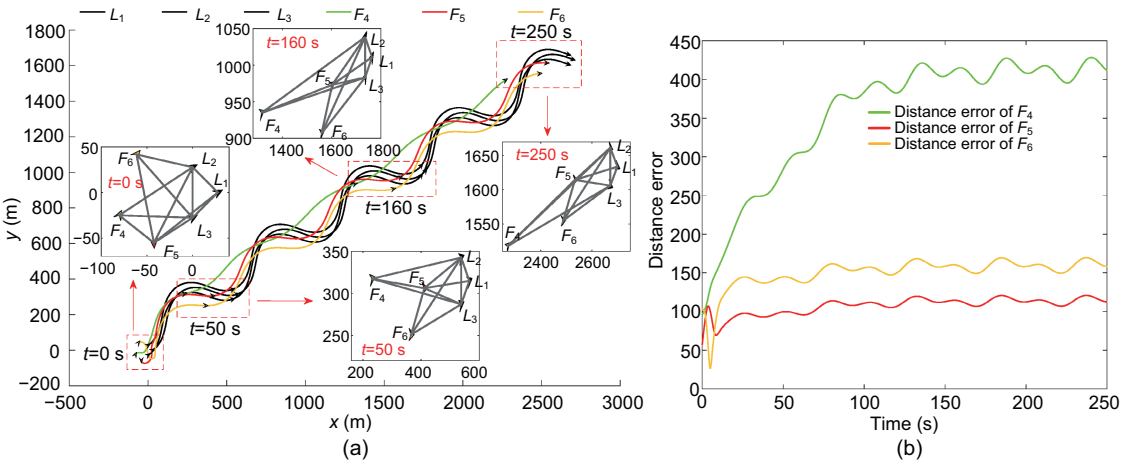

Fig. 6 Formation tracking simulation results under the control law proposed in Zhao SY (2018): (a) trajectories of the six fixed-wing UAVs; (b) tracking errors of the three followers (L: leader; F: follower)

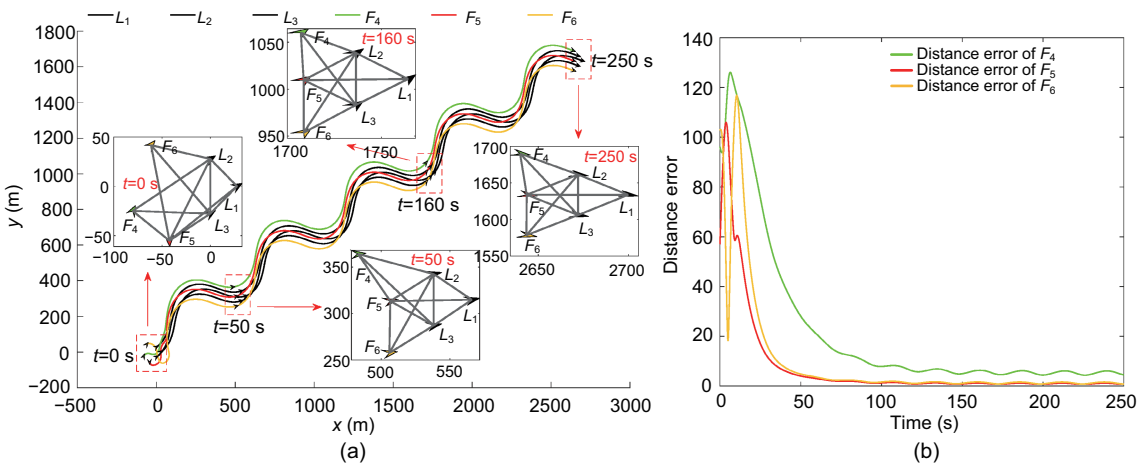

Fig. 7 Formation tracking simulation results under the control law proposed in Xu et al. (2020): (a) trajectories of the six fixed-wing UAVs; (b) tracking errors of the three followers (L: leader; F: follower)

distributed formation tracking control strategy was designed based on the stress matrix. Based on the leader-follower control strategy, the leaders used the predesigned formation information to fly at a desired state and to determine the target configuration; the followers were driven by the affine formation control laws to track the leaders along different trajectories and to converge to the target positions. The Lyapunov theory was applied to analyze the stability of

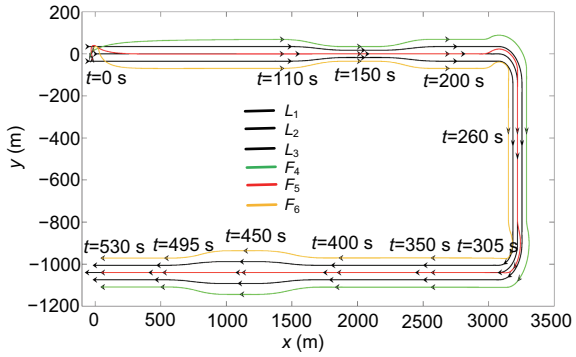

Fig. 8 A simulation example to illustrate the affine transformations of the six fixed-wing UAVs, including translation, zooming in, zooming out, and shearing

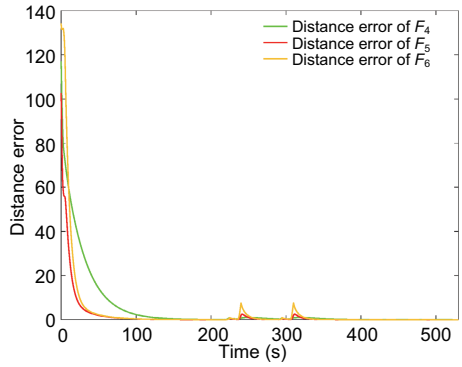

Fig. 10 Tracking errors of the three following fixed-wing UAVs in the formation during affine transformation (F: follower)

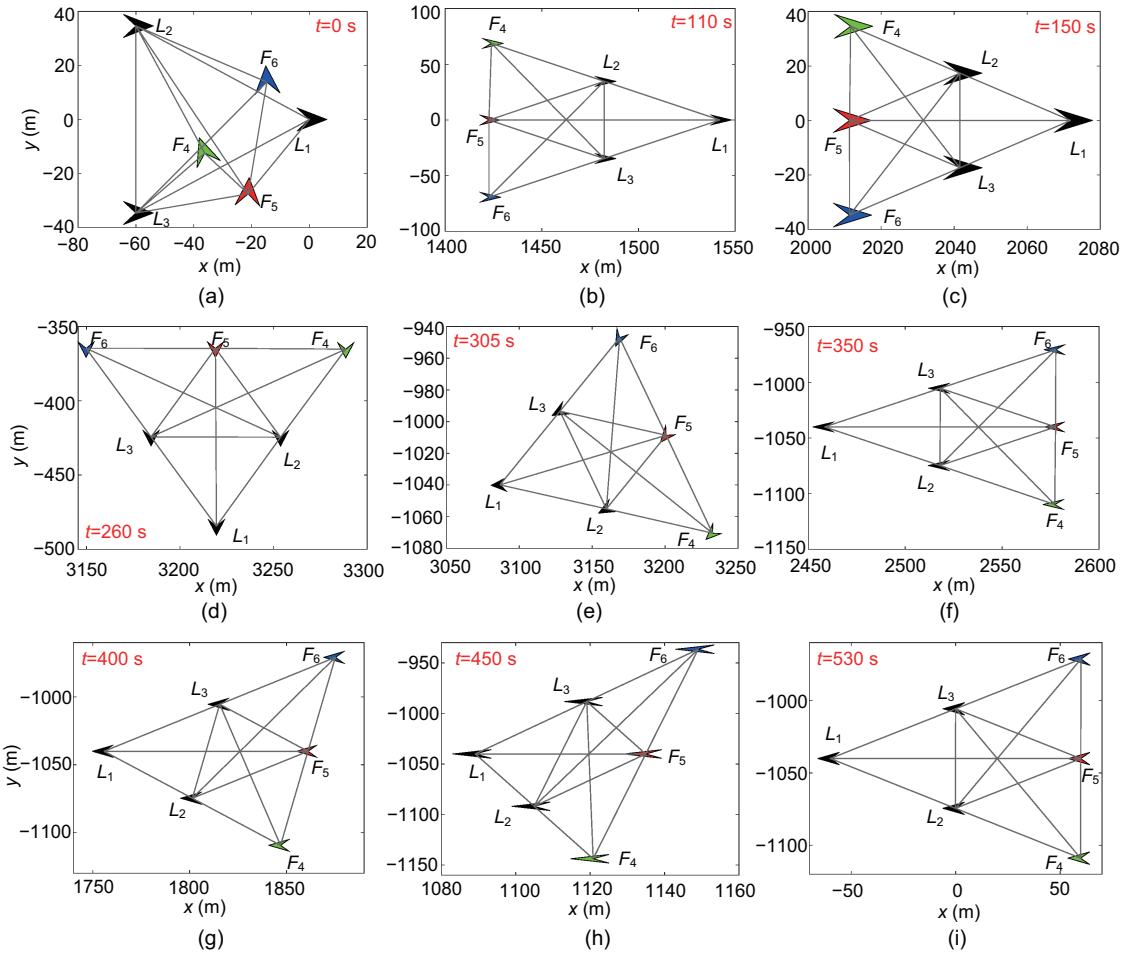

Fig. 9 Six fixed-wing UAVs with affinely transformed nominal configuration at t=0 s (a), 110 s (b), 150 s (c), 260 s (d), 305 s (e), 350 s (f), 400 s (g), 450 s (h), and 530 s (i) (L: leader; F: follower)

the control laws, and a saturated control strategy was proposed to ensure that the speed constraints of fixed-wing UAVs are satisfied. Simulation results showed that the proposed control strategy can adapt well to diverse trajectories and time-varying affine formations. In the future, it is necessary to analyze the convergence of the nonlinear system with input constraints.

Contributors

Huiming LI designed the research and drafted the paper. Hao CHEN and Xiangke WANG helped organize the paper. All the authors revised and finalized the paper.

Compliance with ethics guidelines

Huiming LI, Hao CHEN, and Xiangke WANG declare that they have no conflict of interest.

References

Beard RW, Ferrin J, Humpherys J, 2014. Fixed wing UAV path following in wind with input constraints. *IEEE Trans Contr Syst Technol*, 22(6):2103-2117. https://doi.org/10.1109/TCST.2014.2303787

Chen H, Wang XK, Shen LC, et al., 2021. Formation flight of fixed-wing UAV swarms: a group-based hierarchical approach. *Chin J Aeronaut*, 34(2):504-515. https://doi.org/10.1016/j.cja.2020.03.006

Chen LM, Mei J, Li CJ, et al., 2020. Distributed leader-follower affine formation maneuver control for high-order multiagent systems. *IEEE Trans Autom Contr*, 65(11):4941-4948. https://doi.org/10.1109/TAC.2020.2986684

Connelly R, 2005. Generic global rigidity. *Disc Comput Geom*, 33(4):549-563. https://doi.org/10.1007/s00454-004-1124-4

Fathian K, Summers TH, Gans NR, 2018. Distributed formation control and navigation of fixed-wing UAVs at constant altitude. Int Conf on Unmanned Aircraft Systems, p.300-307. https://doi.org/10.1109/ICUAS.2018.8453462

Lin YJ, Lin ZY, Sun ZY, et al., 2021. A unified approach for finite-time global stabilization of affine, rigid and translational formation. *IEEE Trans Autom Contr*, early access. https://doi.org/10.1109/TAC.2021.3084247

Lin ZY, Wang LL, Chen ZY, et al., 2016. Necessary and sufficient graphical conditions for affine formation control. *IEEE Trans Autom Contr*, 61(10):2877-2891. https://doi.org/10.1109/TAC.2015.2504265

Liu ZH, Wang XK, Shen LC, et al., 2020. Mission-oriented miniature fixed-wing UAV swarms: a multilayered and distributed architecture. *IEEE Trans Syst Man Cybern Syst*, 52(3):1588-1602. https://doi.org/10.1109/TSMC.2020.3033935

Miao ZQ, Liu YH, Wang YN, et al., 2018. Distributed estimation and control for leader-following formations of nonholonomic mobile robots. *IEEE Trans Autom Sci Eng*, 15(4):1946-1954. https://doi.org/10.1109/TASE.2018.2810253

Oh KK, Park MC, Ahn HS, 2015. A survey of multi-agent formation control. *Automatica*, 53:424-440. https://doi.org/10.1016/j.automatica.2014.10.022

Onuoha O, Tnunay H, Ding ZT, 2019a. Affine formation maneuver control of multi-agent systems with triple-integrator dynamics. American Control Conf, p.5334-5339. https://doi.org/10.23919/ACC.2019.8814353

Onuoha O, Tnunay H, Li ZH, et al., 2019b. Optimal affine formation control of linear multi-agent system. IEEE 15th Int Conf on Control and Automation, p.851-856. https://doi.org/10.1109/ICCA.2019.8900001

Paranjape AA, Chung SJ, Kim K, et al., 2018. Robotic herding of a flock of birds using an unmanned aerial vehicle. *IEEE Trans Robot*, 34(4):901-915. https://doi.org/10.1109/TRO.2018.2853610

Ren W, Beard RW, Atkins EM, 2007. Information consensus in multivehicle cooperative control. *IEEE Contr Syst Mag*, 27(2):71-82. https://doi.org/10.1109/MCS.2007.338264

Wang XK, Shen LC, Liu ZH, et al., 2019. Coordinated flight control of miniature fixed-wing UAV swarms: methods and experiments. *Sci China Inform Sci*, 62(11):212204. https://doi.org/10.1007/s11432-018-9887-5

Wang YZ, Shan M, Wang DW, 2020. Motion capability analysis for multiple fixed-wing UAV formations with speed and heading rate constraints. *IEEE Trans Contr Netw Syst*, 7(2):977-989. https://doi.org/10.1109/TCNS.2019.2929658

Wu S, 2013. Aircraft motion equation. In: Song SJ (Ed.), Aircraft Fight Control System. Beihang University Press, Beijing, China (in Chinese).

Xu Y, Zhao SY, Luo DL, et al., 2018. Affine formation maneuver control of linear multi-agent systems with undirected interaction graphs. IEEE Conf on Decision and Control, p.502-507. https://doi.org/10.1109/CDC.2018.8619540

Xu Y, Li DY, Luo DL, et al., 2019a. Affine formation maneuver tracking control of multiple second-order agents with time-varying delays. *Sci China Technol Sci*, 62(4):665-676. https://doi.org/10.1007/s11431-018-9328-2

Xu Y, Luo DL, Li DY, et al., 2019b. Target-enclosing affine formation control of two-layer networked spacecraft with collision avoidance. *Chin J Aeronaut*, 32(12):2679-2693. https://doi.org/10.1016/j.cja.2019.04.016

Xu Y, Li DY, Luo DL, et al., 2019c. Two-layer distributed hybrid affine formation control of networked Euler-Lagrange systems. *J Franklin Inst*, 356(4):2172-2197. https://doi.org/10.1016/j.jfranklin.2018.11.029

Xu Y, Lin ZY, Zhao SY, 2020. Distributed affine formation tracking control of multiple fixed-wing UAVs. 39th Chinese Control Conf, p.4712-4717. https://doi.org/10.23919/CCC50068.2020.9188925

Zhao SL, Wang XK, Lin ZY, et al., 2020. Integrating vector field approach and input-to-state stability curved path following for unmanned aerial vehicles. *IEEE Trans Syst Man Cybern Syst*, 50(8):2897-2904. https://doi.org/10.1109/TSMC.2018.2839840

Zhao SY, 2018. Affine formation maneuver control of multiagent systems. *IEEE Trans Autom Contr*, 63(12):4140-4155. https://doi.org/10.1109/TAC.2018.2798805